Laser speckle contrast imaging in biomedical optics

David A. Boas
Harvard Medical School
Massachusetts General Hospital
Anthinoula A. Martinos Center for Biomedical Imaging
149 13th Street
Charlestown, Massachusetts 02129

Andrew K. Dunn
The University of Texas at Austin
Department of Biomedical Engineering
1 University Station, C0800
Austin, Texas 78712

Abstract. First introduced in the 1980s, laser speckle contrast imaging is a powerful tool for full-field imaging of blood flow. Recently laser speckle contrast imaging has gained increased attention, in part due to its rapid adoption for blood flow studies in the brain. We review the underlying physics of speckle contrast imaging and discuss recent developments to improve the quantitative accuracy of blood flow measures. We also review applications of laser speckle contrast imaging in neuroscience, dermatology and ophthalmology. [DOI: 10.1117/1.3285504]

Keywords: laser speckle contrast; blood flow; biomedical imaging.

Paper 09230SSR received Jun. 8, 2009; revised manuscript received Jul. 20, 2009; accepted for publication Jul. 29, 2009; published online Jan. 13, 2010.

1 Introduction

When a photon scatters from a moving particle, its carrier frequency is Doppler shifted. By analyzing the Doppler shift of the photon, or the distribution of Doppler shifts from a distribution of photons, it is possible to discern the dynamics of the particles scattering the light. Analogously, when coherent light scatters from a random medium, the scattered light produces a random interference pattern called speckle. Movement of scattering particles within the random medium causes phase shifts in the scattered light and thus changes the random interference pattern, producing temporal fluctuations in the speckle pattern that is analogous to the intensity fluctuations that arise from Doppler shifts. The theoretical basis for analyzing speckle intensity fluctuations dates back to the late 1960s with the development of dynamic light scattering.[1,2] There was extensive activity in the 1970s rigorously relating speckle temporal dynamics to various forms of particle dynamics in dilute single-scattering suspensions.[3–5] Extensions to highly scattering systems was made in the 1980s in various guises by Bonner and Nossal[6] and Pine et al.[7] While providing detailed information about system dynamics, these methods were slow at obtaining images of blood flow.[8,9] A solution was presented in the 1980s using a camera to obtain a quick snapshot image of a time-integrated speckle pattern,[10] from which blood flow in the retina was estimated from the spatial statistics of the speckle pattern. This method, laser speckle contrast imaging (LSCI), was advanced in the 1990s for imaging blood flow in the retina and skin with the availability of faster digital acquisition and processing technologies.

In the last decade, there has been an accelerated adoption of the technology as the neuroscience community has used it to measure blood flow in the brain, starting with Ref. 11. During the last eight years, there have been more than 100 publications on the topic, significantly advancing the theory and application of laser speckle imaging. Bandyopadhyay et al.[12] presented an important correction in the calculation of laser speckle contrast and its relation to temporal fluctuations. An important calibration procedure for handling static scattering (from the skull, for instance) that would otherwise confound the estimate of blood flow from spatial laser speckle contrast was developed,[13,14] while Li et al.[15] showed that temporal laser speckle contrast imaging (TLSCI) is intrinsically less sensitive to static scattering. Recently, Kirkpatrick et al.[16] and Duncan et al.,[17] presented important theoretical efforts quantifying the impact of speckle size and sampling windows on the statistics of laser speckle, and others have demonstrated more efficient algorithms for calculating speckle contrast to enable real-time visualization.[18,19] Finally, LSCI is being implemented in multimodal imaging schemes to obtain additional information about the tissue.[20–23]

In the next sections, we review the theoretical background of speckle contrast and the important considerations when using spatial speckle contrast or temporal speckle contrast to estimate blood flow. We then review several of the application areas for LSCI that have been advancing over the last twenty years, including imaging blood flow in the retina, skin, and the brain.

2 Theoretical Background

2.1 *Speckle Basics*

Speckle arises from the random interference of coherent light. Whenever coherent light interacts with a random scattering medium, a photodetector will receive light that has scattered from varying positions within the medium and will have thus traveled a distribution of distances, resulting in constructive and destructive interference that varies with the arrangement of the scattering particles with respect to the photodetector. Thus, if this scattered light is imaged onto camera, we will see that the interference varies randomly in space, producing a randomly varying intensity pattern known as speckle. If scattering particles are moving, this will cause fluctuations in the interference, which will appear as intensity variations at the photodetector. The temporal and spatial statistics of this speckle pattern provide information about the motion of the scattering particles. The motion can be quantified by measur-

Address all correspondence to: David A Boas, Harvard Medical School, Massachusetts General Hospital, Anthinoula A. Martinos Center for Biomedical Imaging, 149 13th Street, Charlestown, Massachusetts 02129. Tel: 617-724-0130; Fax: 617-643-5136; E-mail: dboas@nmr.mgh.harvard.edu

1083-3668/2010/15(1)/011109/12/$25.00

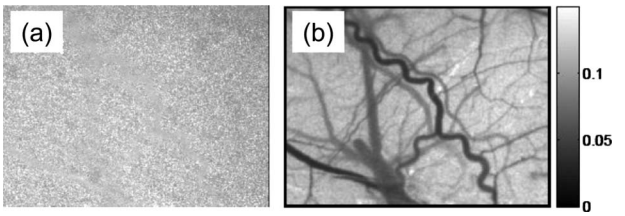

Fig. 1 (a) Raw speckle image from the thin skull of a rat, showing a grainy pattern in which it is possible to discern some spatial variation in the speckle contrast, and (b) when the spatial speckle contrast is estimated from a 7×7 window of pixels, the blood vessels on the surface of the brain become apparent with high spatial resolution.

ing and analyzing either the temporal variations[4] or the spatial variations.[10] Using the latter approach, 2-D maps of blood flow can be obtained with very high spatial and temporal resolution by imaging the speckle pattern onto a CCD camera and quantifying the spatial blurring of the speckle pattern that results from blood flow. In areas of increased blood flow, the intensity fluctuations of the speckle pattern are more rapid, and when integrated over the CCD camera exposure time (typically 1 to 10 ms), the speckle pattern becomes blurred in these areas. By acquiring an image of the speckle pattern and quantifying the blurring of the speckles in the image by measuring the spatial contrast of the intensity variations, spatial maps of relative blood flow can be obtained.[24] Alternatively, instead of measuring the spatial contrast of the speckle pattern, one can measure the temporal contrast.[15,25,26] Each has its advantages and disadvantages, as we detail further in the following. In short, spatial contrast offers superior temporal resolution at the expense of spatial resolution and vice versa for temporal contrast, while the advantages of both can be obtained with spatiotemporal algorithms.[17,26]

To quantify the blurring of the speckles, the speckle contrast, defined as the ratio of the standard deviation to the mean intensity, is computed as,[24]

$$K_s = \frac{\sigma_s}{\langle I\rangle}. \tag{1}$$

Note that we use σ_s to refer to the spatial standard deviation of the speckle intensity and σ_t to refer to the temporal standard deviation. Similarly for the spatial speckle contrast K_s and the temporal speckle contrast K_t. A typical example of a raw speckle image of the rat cortex, taken through a thinned skull, and the computed spatial speckle contrast are shown in Fig. 1 under normal conditions. The raw speckle image illustrates the grainy appearance of the speckle pattern. The speckle contrast image, computed directly from the raw speckle image using Eq. (1), represents a 2-D map of blood flow. Areas of higher baseline flow, such as large vessels, have lower speckle contrast values and appear darker in the speckle contrast images.

Theoretically, the speckle contrast has values between 0 and 1, provided that the speckle pattern is fully evolved. A speckle pattern is considered fully evolved provided that the phases of the interfering electromagnetic fields are uniformly distributed, as can be verified by confirming a negative exponential probability distribution of the speckle intensity pattern.[17,27] A spatial speckle contrast of 1 indicates that there is no blurring of the speckle pattern and therefore, no motion, while a speckle contrast of 0 means that the scatterers are moving fast enough to blur all of the speckles. The speckle contrast is a function of the exposure time T of the camera and is related to the autocovariance of the intensity fluctuations in a single speckle $C_t(\tau)$ by[10]

$$K^2 = \frac{\sigma_s^2(T)}{\langle I\rangle^2} = \frac{1}{T\langle I\rangle^2}\int_0^T C_t(\tau)\mathrm{d}\tau, \tag{2}$$

although it has recently been indicated that the proper calculation of a second moment is[12]

$$\frac{\sigma_s^2(T)}{\langle I\rangle^2} = \frac{1}{T^2\langle I\rangle^2}\int_0^T\int_0^T C_t(\tau-\tau')\mathrm{d}\tau\,\mathrm{d}\tau' = \frac{2}{T\langle I\rangle^2}\int_0^T\left(1-\frac{\tau}{T}\right)C_t(\tau)\mathrm{d}\tau. \tag{3}$$

While Eq. (3) is the correct formulation and should be used in data analysis, it appears to produce insignificant differences in biomedical applications when considering relative changes in blood flow and the integration time is sufficiently long.[14,28,29]

The autocovariance is defined as

$$C_t(\tau) = \langle[I(t)-\langle I\rangle_t][I(t+\tau)-\langle I\rangle_t]\rangle_t, \tag{4}$$

where $\langle\cdots\rangle_t$ indicates a time-averaged quantity. It is convenient to consider that the intensity temporal autocorrelation function $g_2(\tau)$ and its relation to the autocovariance since $g_1(\tau)$ has been calculated[5] explicitly for a wide range of dynamically varying media in the dynamic light scattering community for the last 30 yr.[5] The temporal autocovariance function is related to the autocovariance by

$$g_2(\tau) = 1 + \frac{C_t(\tau)}{\langle I\rangle_t^2}, \tag{5}$$

$$g_2(\tau) = 1 + \beta|g_1(\tau)|^2, \tag{6}$$

where $g_1(\tau)$ is the electric field temporal autocorrelation function given by

$$g_1(\tau) = \langle E(t)E^*(t+\tau)\rangle/\langle E(t)E^*(t)\rangle. \tag{7}$$

Note that the average in Eq. (7) is an ensemble average that is only equivalent to a temporal average for ergodic systems (i.e., systems that evolve through all ensembles or arrangements over time). Equation (6) is widely known as the Siegert relation, where β accounts for loss of correlation related to the ratio of the detector size to the speckle size and polarization. If the source is polarized and the detector is not, then β=0.5. A detailed discussion and derivation of the value of β can be found in Ref. 30. Note that the coherence length of the light must be longer than the width of the distribution of detected photon path lengths through the scattering medium such that all detected photons will interfere coherently. If the coherence length is comparable to or less than this distribution width, then the relation in Eq. (6) is not valid and the

calculation of the speckle contrast becomes extremely complex.[31]

Starting with the first paper on laser speckle flowmetry,[10] it has been common to assume that the field temporal autocorrelation function has the form

$$g_1(\tau) = \exp\left(-\frac{\tau}{\tau_c}\right). \tag{8}$$

This gives a speckle contrast

$$K = \beta^{0.5}\left\{\frac{\tau_c}{T} + \frac{\tau_c^2}{2T^2}\left[\exp\left(-\frac{2T}{\tau_c}\right) - 1\right]\right\}^{0.5}, \tag{9}$$

where the correlation time τ_c is assumed to be inversely proportional to a measure of the speed or flow of the scattering particles.[24] As in the case of laser Doppler measurements, it is theoretically possible to relate the correlation times τ_c to the absolute speed of the red blood cells, but this is difficult to do in practice since the number of moving particles that the light interacts with and their orientations are unknown.[6,24] However, relative spatial and temporal measures of speed can be easily obtained from the ratios of the correlation times. Note the reminder from Ref. 12 that the form in Eq. (8) is related only to speed in the highly scattering regime where photons have each experienced multiple scattering events from moving particles. In the single dynamic scattering regime, when photons scatter no more than once from moving particles, then the argument of the exponent in Eq. (8) should be squared to represent blood speed. In the single dynamic scattering regime, Eq. (8) is correct if the moving particles are undergoing Brownian motion.[12] Further, the relation between τ_c and the speed of the scattering particles depends on the speed distribution of the scattering particles sampled by the detected light, a topic that is receiving increased attention in the speckle contrast community.[28,29,32] Finally, the speckle contrast literature tends to use speed and flow interchangeably when the speed is a length per unit time, while flow is a volume per unit time. While the theoretical derivation suggests that speckle contrast is measuring speed, it is possible that sensitivity to the number of moving particles would render speckle contrast a measure of flow, as has been rigorously shown for laser Doppler blood flowmetry[6] and suggested by some LSCI studies.[11] A rigorous analysis of this question is needed.

As indicated by Eq. (9), the speckle contrast is a function of the camera exposure time T and the time scale of the sample dynamics τ_c. As the exposure time goes to zero, the spatial speckle contrast approaches a value of 1. As the exposure time becomes long compared to τ_c, the speckle contrast approaches a value of 0. At both extremes, the speckle contrast will not be sensitive to spatial or temporal variations in the speckle contrast. As detailed in Yuan et al.,[33] the sensitivity to and contrast to noise ratio for variations in the speckle contrast is optimized for $T \approx \tau_c$, falling sharply for shorter T and gradually for longer T (see Fig. 2, reproduced from Ref. 33 with permission). As discussed by Duncan and Kirkpatrick,[28] we are assuming that the τ_c related to blood flow is significantly shorter than the correlation time of any other dynamic processes within the sample, such as Brownian motion.

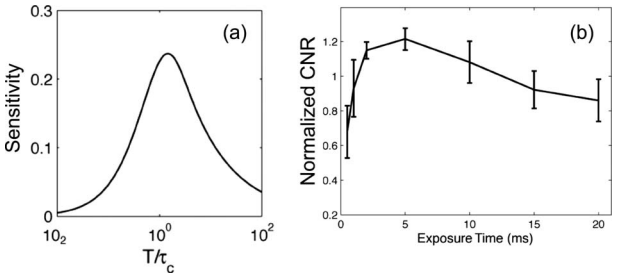

Fig. 2 (a) Speckle contrast sensitivity to particle dynamics as given by camera integration time divided by decorrelation time and (b) the normalized contrast-to-noise ratio of changes in speckle contrast versus camera integration time due to changes in rodent cerebral blood flow. Reproduced from Ref. 33 with permission.

2.2 *Spatial Speckle Contrast*

2.2.1 *Effect of speckle size and window size*

Accurate estimation of the speckle contrast from the spatial statistics of the speckle pattern generally assumes that the speckle intensity distribution follows a negative exponential probability distribution function.[17,27,34] We always mentioned that one requirement for this is that the speckle pattern be fully evolved, i.e., that the received light have an effectively uniform phase distribution. Additionally, care must be taken in spatial sampling of the speckle pattern. Specifically, the speckle size relative to the camera pixel size must be considered as well as the number of pixels that are used to estimate the speckle contrast.

Typically, the speckle pattern is imaged onto a camera in which case the minimum speckle size will be given by

$$\rho_{\text{speckle}} = 2.44\lambda(1+M)f/\#, \tag{10}$$

where λ is the wavelength of light, M is the magnification of the imaging system, and $f/\#$ is the f number of the system. As shown by Kirkpatrick et al.,[16] the Nyquist sampling criteria must be satisfied by having the minimum speckle size be two times larger than the camera pixel size, i.e., $\rho_{\text{speckle}} \geqslant 2\rho_{\text{pixel}}$, to obtain a negative exponential distribution. It has been commonly stated that the speckle size should match the pixel size, but as indicated by Ref. 16, this results in a slight distortion of the intensity distribution function with the result that the speckle contrast is underestimated by approximately 20% (see Fig. 3, reproduced from Ref. 16 with permission). Underestimating the speckle contrast, if not calibrated, will result in a systematic error in the estimated correlation time τ_c and the associated sample dynamics. This reduction in speckle contrast is absorbed by β in Eq. (9) and can be easily estimated empirically for calibrating the speckle contrast measurement.[13] However, any reduction in β, despite calibration, does reduce sensitivity to spatial and temporal variations in the speckle contrast. Additionally, the distortion in the intensity distribution function likely produces systematic errors in the estimated sample dynamics, but the magnitude of these errors remains to be estimated.

Speckle contrast is estimated from the mean and standard deviation of the speckle intensity, which are generally determined from a square region of N_{pixels} (i.e., $N_{\text{pixels}}^{1/2} \times N_{\text{pixels}}^{1/2}$). Clearly a larger value of N_{pixels} will give a more accurate

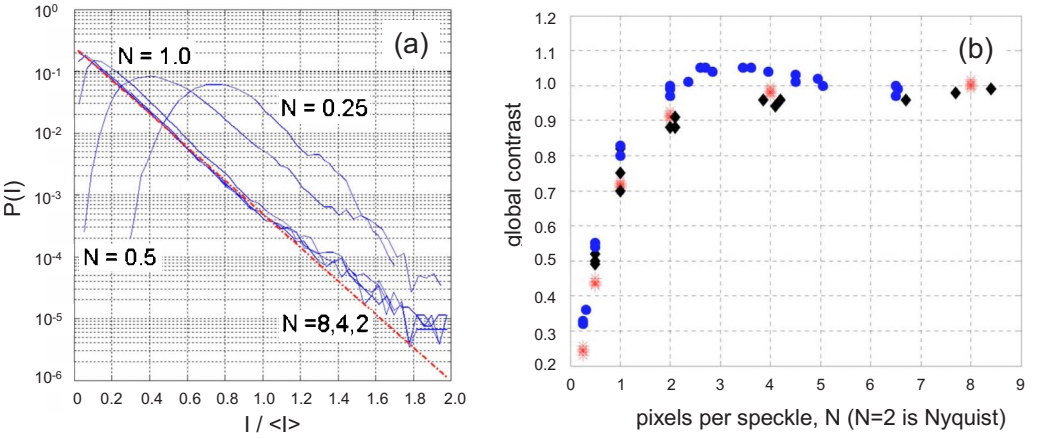

Fig. 3 (a) Speckle intensity probability distribution function considering different numbers of pixels per speckle N and the distribution is an exponential for $N=2$. (b) The speckle contrast for a static medium equals its expected value of 1 when $N=2$. Reproduced from Ref. 16 with permission.

estimate of the speckle contrast, but at the expense of spatial resolution. If the window size is too small, then the large variation in the estimate of the speckle contrast will reduce sensitivity to vascular variations. A survey of the literature indicates that the community has empirically settled on a window size of 7×7 pixels as a reasonable trade-off between spatial resolution and uncertainty in the estimated speckle contrast, but this all depends on camera resolution, speckle size, and desired contrast resolution.

Duncan et al.[17] recently presented an important analysis that formulated the dependence of the mean speckle contrast and variation in the estimated speckle contrast as a function of the window size. Assuming that the Nyquist sampling criterion is met, they determined that the variation of the estimated speckle contrast could be expressed by a dimensionless width parameter σ_g as

$$\sigma_g = 1 + 0.454p^{0.672}N_{\text{pixels}}^{-0.373}, \tag{11}$$

where $p=\rho_{\text{speckle}}/\rho_{\text{pixel}}$ is the number of pixels per speckle. Their formulation reveals that the variation in the speckle contrast dramatically decreases as the window size is increased to 7×7, but then diminishing returns are obtained for larger window sizes, i.e., a 7×7 window sits near the bend in the curve (see Fig. 9 in Ref. 17). Note that the variation in the estimated speckle contrast is a strong function of the number of pixels per speckle. Essentially, increasing the speckle size means that a given window of N_{pixels} is estimating the speckle contrast from fewer speckles. Finally, smaller window sizes result in an underestimation of the speckle contrast (see Fig. 8 in Ref. 17).

2.2.2 *Effect of static scattering*

It is important to consider the effect of static scattering on the estimate of the sample dynamics from the speckle contrast. A purely static component to the scattered electric field will produce a speckle contrast that remains constant as the camera integration time is increased. If this effect is not considered, then it results in an underestimation of the spatial and temporal variations in the sample dynamics.[13–15,35] Consider a scattered electric field reaching the detector of the form

$$E(t) = E_f(t)\exp(-i\omega t) + E_s\exp(-i\omega t), \tag{12}$$

where $E_f(t)$ is the fluctuating electric field scattered from moving particles, E_s is the static electric field scattered from nonmoving particles, and $\omega=2\pi v/\lambda$ is the angular frequency of the electric field related to the wavelength λ and speed v of light in the sample. Substituting into Eq. (6) and Eq. (7) gives an intensity temporal autocorrelation function of

$$g_2(\tau) = 1 + \beta[\rho^2|g_{1,f}(\tau)|^2 + 2\rho(1-\rho)|g_{1,f}(\tau)| + (1-\rho)^2] + C_{\text{noise}}^2, \tag{13}$$

where $\rho=I_f/(I_f+I_s)$, $I_f=\langle E_fE_f^*\rangle$ is the time-averaged intensity of the fluctuating dynamically scattered light, $I_s=E_sE_s^*$ is the intensity of the statically scattered light, and $g_{1,f}(\tau)=\langle E_f(t)E_f^*(t+\tau)\rangle/\langle E_f(t)E_f^*(t)\rangle$. C_{noise} is a term added to account for contrast that arises from measurement noise such as shot noise or camera readout noise.[13,14] We can now obtain a new formulation for the speckle contrast by substituting Eq. (13) into Eq. (3) and assuming an exponential decay for $g_1(\tau)$ [Eq. (8)],

$$K = \beta^{0.5}\left[\rho^2\frac{\exp(-2x)-1+2x}{2x^2} + 4\rho(1-\rho)\frac{\exp(-x)-1+x}{x^2} + (1-\rho)^2\right]^{0.5} + C_{\text{noise}}, \tag{14}$$

where $x=T/\tau_c$.

The implications of Eq. (14) are straightforward. If the relative contributions of the fluctuating signal I_f and the static signal I_s expressed by ρ are unknown, then it is not possible to estimate the dynamics of the sample τ_c. A simple multiexposure calibration scheme was proposed by Refs. 13 and 14. Briefly, performing measurements on a static sample with the same light source and imaging optics provides an estimate of β. Similarly, β can be estimated on the sample of interest by obtaining a measurement with $T\ll\tau_c$. Measurements on the sample with $T\gg\tau_c$ drive the first two terms of Eq. (14) to

zero, providing an estimate of $(1-\rho)$. Care is taken in these two measurements to estimate C_{noise} or to ensure that it is negligible. Finally, measurements can be made with multiple intermediate T's or the optimal $T \approx \tau_c$ to then estimate the spatial and temporal variations of τ_c within the sample. From the relative variations in τ_c we then obtain relative measures of flow.

2.3 *Temporal Speckle Contrast*

Laser Doppler blood flowmetry is based on measuring the temporal fluctuations of speckle with sufficient temporal resolution to resolve the power spectrum of the intensity fluctuations, which forms a Fourier transform pair with the intensity temporal autocorrelation function[1,6] $g_1(\tau)$. This requires a temporal sampling resolution of more than 20 kHz for superficial measurements and 10 MHz for deeper tissues, as measured with diffuse correlation spectroscopy. The high data bandwidth limits measurements to a few points in space at a given time precluding rapid imaging.[8,9] TLSCI, on the other hand, images the time-integrated speckle and subsamples its temporal variation at 10 Hz or faster.[15,25,26] In this way, it images all pixels in parallel but does not resolve the high-frequency temporal variation. Instead, it obtains the temporal speckle contrast K_t from the temporal standard deviation σ_t of the speckle intensity divided by the mean intensity. This temporal speckle contrast can then be related to the sample dynamics via Eq. (9). By using temporal sampling to estimate the speckle contrast, rather than spatial sampling, one maintains a higher spatial resolution but at the expense of temporal resolution.

A rigorous analysis of the effect of speckle size and number of samples on K_t has not been published. Cheng et al. showed in Fig. 3 of Ref. 25 that K_t correlated well with the true speed when estimated from 15 or more independent samples of the speckle intensity. This is significantly fewer than the minimum of 49 that is required in a 7×7 window to estimate the spatial speckle contrast with minimal uncertainty.[17] Although a rigorous analysis comparing similar statistical quantities between temporal and spatial contrast is still needed, the temporal analysis is likely to perform better with fewer samples, provided that temporal samples are more statistically independent than the spatial samples. The spatial samples will be correlated because one typically imposes that the speckle size be 2 times greater than the pixel size to satisfy the Nyquist theorem. Temporal samples, on the other hand, will be uncorrelated provided that the sampling time $T_s > \tau_c$. In the exposed rodent brain, $\tau_c \sim 5$ ms, enabling more than 100 statistically independent samples per second.

Temporal speckle contrast appears to be inherently less sensitive to the contribution of static scattering than spatial speckle contrast.[15,32] When estimating speckle contrast from spatial sampling, static scattering has an additive effect in increasing the speckle contrast [see Eq. (14)]. Static scattering does not induce temporal variation in the speckle intensity and therefore will not contribute to the temporal standard deviation σ_t. However, it does contribute to the mean intensity $\langle I\rangle_t = I_f + I_s$ and thus reduces the estimate of the temporal speckle contrast since $K_t = \sigma/\langle I\rangle_t$. While this impacts the ability to quantify an absolute measure of speed from an absolute measure of speckle contrast, it does not prevent estimation of the relative changes since $\langle I\rangle_t$ cancels in the ratio as long as it remains constant. From the relative changes in K_t we can estimate the relative changes in τ_c and subsequently the relative changes in flow.

2.4 *Spatial versus Temporal Speckle Contrast*

Speckle contrast can be estimated from either the spatial statistics or the temporal statistics and related to blood flow. The spatial statistics offers better temporal resolution but at the expense of spatial resolution because of the requirement to use a sufficiently large window of image pixels in the calculation. If the pixel size is too small relative to the speckle size, then speckle contrast will be underestimated and sensitivity to spatial and temporal variations in speckle contrast will degrade. Ideally, the speckle size is twice as large as a pixel and the contrast is estimated from at least $7\times7=49$ pixels. The temporal statistics offer better spatial resolution at the expense of temporal resolution. If temporal samples are statistically independent, i.e., the time between samples is greater than the correlation time, then a minimum of only 15 samples is required to accurately estimate the speckle contrast and have good sensitivity to spatial and temporal variations in speckle contrast. For typical brain applications, the correlation time is approximately 5 ms. Thus, given an image sample every 10 ms, temporal speckle contrast could be estimated every 150 ms with pixel spatial resolution. Compare this with spatial speckle contrast, which can be estimated at the camera frame rate with a resolution of 7×7 pixels. Note that while this spatial resolution difference is important on the surface of the sample, it is quickly blurred by photon scattering beneath the surface of the tissue. The difference in spatial resolution between spatial and temporal statistics likely makes no difference when imaging more than 100 μm in highly scattering tissue.

Spatial and temporal statistics do have important differences when it comes to the treatment of static scattering. Static scattering will produce an additive offset to the spatial speckle contrast. If this is not properly calibrated, then one would overestimate the absolute speckle contrast and underestimate relative changes in the speckle contrast, with the result that both absolute blood flow and relative changes in blood flow would be underestimated. Static scattering does not produce an additive offset in the temporal speckle contrast, but instead scales the speckle contrast by a factor related to the relative contribution of statically and dynamically scattered photons. While this confounds estimates of the absolute speckle contrast, the scale factor generally cancels when estimating relative changes in speckle contrast.

Computational efficiency has plagued the calculation of speckle contrast, usually requiring much more computational time than data acquisition time, thus preventing real-time visualization. While temporal speckle contrast is generally less computationally expensive than spatial speckle contrast,[36] Tom et al.[18] recently developed improved algorithms that enable speckle contrast calculation at rates that exceed image acquisition rates so that the acquisition time is now the limiting factor in the temporal resolution. As a result, true real-time calculations of speckle contrast and blood flow changes are now possible.

3 Applications

The need for high-resolution blood flow imaging spans many applications, tissue types, and diseases. LSCI and related techniques have been used for a large number of blood flow imaging applications in tissues such as the retina, skin, and brain. These tissues are particularly well suited for LSCI since the microvasculature of interest is generally superficial. Because of its measurement geometry LSCI is unable to sense blood flow in deep tissues. One of the earliest uses of speckle imaging was in the retina, where the vasculature and blood flow of interest is accessible.[37,38] More recently, LSCI has become one of the most widely used methods for *in vivo* imaging of blood flow in the brain, particularly in small animal models of both normal and diseased brain.[11] Imaging of cerebral blood flow with LSCI typically requires thinning or removal of a portion of skull to access the cortex. Prior to its application to cerebral blood flow studies, the standard method for *in vivo* blood flow determination in animal models was laser Doppler flowmetry, which typically consists of a fiber optic probe that provides relative blood flow measurements at a single spatial location. Although scanning laser Doppler instruments exist,[8,9] their temporal resolution is limited by the requirement to scan the beam. LSCI instruments on the other hand, enable noncontact full-field imaging of blood flow without requirement any scanning. In addition, the relatively simple instrumentation makes LSCI instruments easy to construct and use. In this section, several applications of LSCI are illustrated.

3.1 *Skin Perfusion*

Full-field monitoring of skin perfusion was one of the earliest uses[24] of LSCI. Initially, skin was a convenient *in vivo* test sample. However, images of skin perfusion are complicated by the fact that the majority of the vasculature is contained beneath a layer of tissue that has few blood vessels. Therefore, it is usually difficult to monitor flow in single vessels in the skin, although LSCI is able to quantify overall perfusion in the capillary bed.[26] Recently Choi et al. have taken advantage of this and demonstrated that LSCI can be used in conjunction with laser therapy for feedback during treatment of port wine stain[39,40] (PWS). In laser therapy of PWS birthmarks, pulsed visible laser light is used to treat vascular lesions. Although laser therapy is now the standard treatment for PWS, some areas of residual perfusion can exist following treatment. LSCI has the potential to provide real-time feedback during PWS treatment by indicating the spatial distribution of perfusion in the skin before and after laser therapy, as illustrated[41] in Fig. 4.

LSCI is also highly effective in quantifying microvascular blood flow in the rodent dorsal skinfold model in which a section of skin is resected and a window is inserted. This preparation enables chronic studies of microvascular structure and function within the tissue under the window. Studies of dermatalogical laser treatments in skin have utilized this preparation as well as a large number of tumor biology studies in which tumors can be implanted in the tissue beneath the window. LSCI has enabled quantification of blood flow changes in individual vessels to be monitored in the dorsal skinfold model.[39]

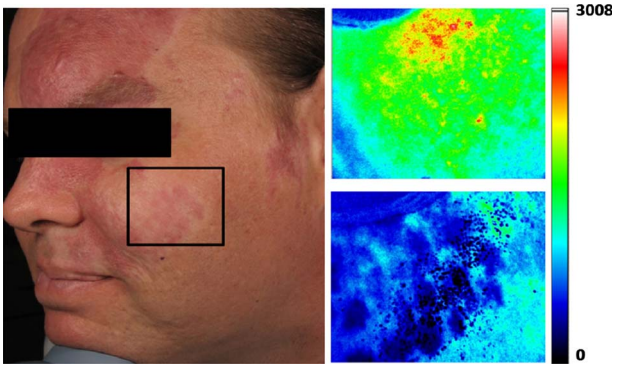

Fig. 4 Illustration of LSCI for monitoring PWS treatment. Left: Photograph of patient with PWS in the area indicated by the rectangle. LSCI images were acquired immediately before (upper) and 15 minutes after (lower) laser therapy. Figure graciously provided by Bernard Choi.

3.2 *Retinal Blood Flow*

Another of the earliest applications of LSCI and related techniques was in visualization and quantification of blood flow in the retina in both animals and humans.[37,38,42] Since the retina is accessible and blood flow is an important indicator in a variety of ophthalmology conditions, considerable effort has been invested in developing blood flow imaging methods for the eye. Speckle-based imaging of retinal blood flow has been performed with diode lasers as well as argon ion lasers that are coupled into fundus cameras. The group of Tamaki et al.[38] have developed a measure called the normalized blur (NB), which is used as an alternative to the speckle contrast, but is still computed from the time-integrated speckle intensity fluctuations. Applications in the retina have included analysis of the effects of a wide range of pharmacological agents on blood flow[43,44] as well as analysis of flow around the optic nerve head.[45] Despite the large number of reports of the use of speckle techniques for measuring retinal blood flow, however, very few images of retinal blood flow in humans have been reported. The majority of studies have reported average flow values that are calculated from images without showing any spatial maps of blood flow. The study by Isono et al.[46] is one of the few publications to show spatial flow maps in the human retina, and these maps were generated by stitching together images from adjacent areas to create a composite image covering a 3-mm^2 area of retina. One reason that many of the earlier human retinal studies neglected to show spatial maps could be that most instruments had limited spatial resolution due to small camera sensors[47] (100×100 pixels).

3.3 *Brain Applications*

For most applications in the brain, a portion of the skull is either thinned or removed and saline or mineral oil is placed on the surface to improve image quality by minimizing the effects of static scattering elements. Most applications in the brain involve quantifying the changes in speckle contrast at each pixel as an indication of the relative cerebral blood flow. Next we summarize applications of this approach to the brain.

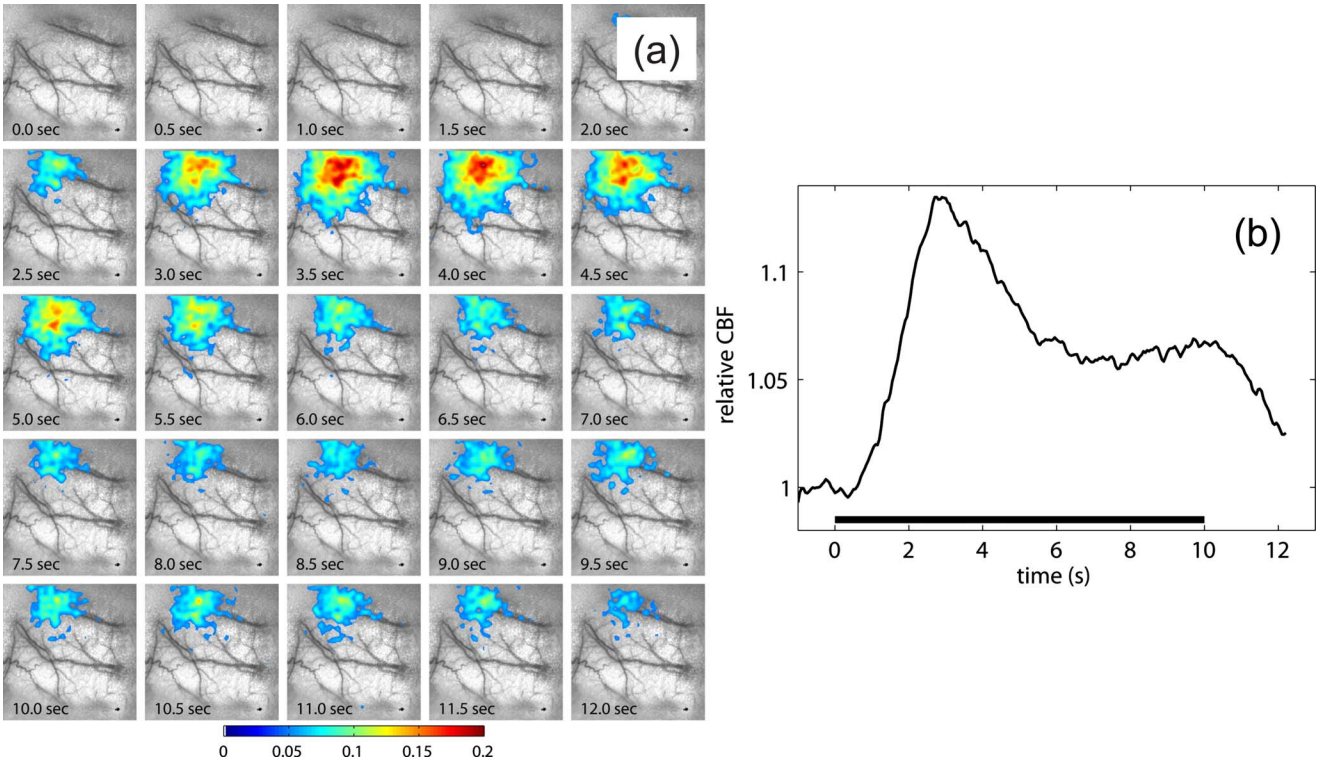

Fig. 5 Imaging of stimulus induced changes in blood flow in the brain. (a) Sequence of images showing the percent changes in blood flow in response to 10 s of forepaw stimulation and (b) graph illustrating the percent change in blood flow over a 1.75×1.75-mm region of interest centered on the activation [see (a)]. Reproduced from Ref. 54 with permission.

3.3.1 *Functional brain activation*

Over the past two decades functional magnetic resonance imaging (fMRI) has become the standard technique for investigating how the brain responds to various types of stimuli.[48] fMRI studies have been widely used in humans as well as animals for both clinical applications and basic research studies. The majority of fMRI studies use BOLD (blood oxygen level dependent) fMRI, whereby the changes in blood oxygenation, in particular deoxyhemoglobin, are detected. Therefore, BOLD fMRI measurements sense the hemodynamic response to brain activation.

Optical techniques are widely used to image the hemodynamic response to various stimuli. In particular, optical imaging of intrinsic signals is commonly used. This method has provided numerous insights into the functional organization of the cortex[49–52] by mapping the changes in cortical reflectance arising from the hemodynamic changes that accompany functional stimulation. The majority of these studies have been based on qualitative mapping at a single wavelength, and while they have provided valuable insight into many aspects of cortical function, the techniques used in these studies have been unable to reveal quantitative spatial information about the individual hemodynamic (hemoglobin oxygenation and volume and blood flow) and metabolic components that underlie the measured signals.

The blood flow changes that accompany brain activation are particularly important in estimating the oxygen consumption of the brain. Laser Doppler flowmetry has been used extensively to quantify the blood flow changes in the somatosensory cortex in response to stimulation in animal models.[53] However, laser Doppler measurements of the blood flow response are limited to single spatial locations due to the relatively fast temporal dynamics of the blood flow response (typically a few seconds). Since LSCI does not require any scanning, full-field imaging is possible with high temporal resolution that is sufficient to resolve the blood flow dynamics due to functional activation in the normal brain.[20,54–56]

An illustration of the ability of LSCI to image the spatiotemporal changes in cerebral blood flow (CBF) following functional activation is given in Fig. 5. A 5×5-mm area of cortex was imaged in a rat through a thinned skull as the forepaw of the rat was stimulated with electrical pulses. The stimulus was applied for 10 s (0.5 mA) and 20 trials were repeated. The speckle contrast images at each time, relative to the stimulus were averaged. Speckle contrast values were converted to speckle correlation decay times (τ_c) at each pixel in all images, and ratios of the inverse of the decay times were used as a measure of the relative changes in CBF.

Figure 5 highlights the strength of LSCI in revealing both the spatial and the temporal blood flow dynamics. A series of images are shown at 0.5-s intervals, and illustrate a localized increase in CBF beginning approximately 1 s after stimulation onset. The relative changes in CBF are shown superimposed on the vasculature (derived from the speckle contrast image) and the changes in CBF are displayed for all pixels with an increase in CBF greater than 5%. The time course of the CBF changes averaged over a region of interest centered on the activated area illustrates a peak increase in CBF of approximately 12% occurring 3 s after stimulus onset. The initial peak in CBF then decreases to approximately half of its

maximum amplitude to a value of ~6%, where it remains until the end of the stimulus, in a manner consistent with previous laser Doppler measurements of CBF during extended forepaw stimulation.[57] This time course also reveals the very high SNR of LSCI for relative CBF measurements.

Since the CBF response to functional activation is only one component of the overall hemodynamic response, a number of groups have combined LSCI with other optical techniques to simultaneously measure CBF and other hemodynamic and metabolic parameters. Because the wavelength used for LSCI can lie anywhere in the red or near-IR regions, LSCI can be performed simultaneously with other techniques such as multispectral reflectance imaging (MSRI) of hemoglobin oxygenation and blood volume,[20,54,58] fluorescence imaging of NADH and flavoproteins,[55] and phosphorescence quenching measurements of the partial pressure of oxygen.[21] For example, by adding a second camera and light source to the LSCI setup, LSCI and MSRI can be performed simultaneously.[59] For MSRI, incoherent light of different wavelengths (typically 550 to 650 nm) sequentially illuminates the cortex, while longer wavelength laser light (700 to 800 nm) is used for speckle imaging. The reflected light from each source is spectrally separated and two cameras are used to record the speckle and multispectral signals. For MSRI, each set of spectral images can then be converted to changes in oxyhemoglobin (HbO) and deoxyhemoglobin (HbR) at each pixel to yield maps of hemoglobin changes, while LSCI images are processed as already described.

3.3.2 *Cortical spreading depression and migraine headache*

Cortical spreading depression [or spreading depolarization (SD)] is a wave of negative potential shift that slowly propagates across the cortex at a rate of 2 to 5-mm/min, and was first identified in rabbits in 1944 by Leao.[60] SD is associated with large ionic shifts, increased metabolism, and hemodynamic changes. SD has been studied extensively for more than 50 yr and its role in the pathophysiology of stroke, migraine, and subarachnoid hemorrhage is well established.[61,62] Recent clinical studies have further emphasized the importance of SD in human stroke and brain injury.[63–66] Despite this, the physiologic changes that occur during SD are not fully understood. In particular, the role of cerebral microcirculation on the impact of SD on brain tissue is poorly understood. In animal models, SD can be induced in normal brain through topical application of KCl or through localized injury such as pinprick. Once induced, SD propagates across the cortex and is associated with large transient changes in dc potential. In response to the increased metabolism required for cells to repolarize, SD is typically accompanied by a large transient increase in blood flow (hyperemia).

SD was one of the first applications of LSCI in the brain.[11,20,67] Laser Doppler flowmetry had been used to quantify the temporal changes in CBF for many years, and laser Doppler was suitable for quantifying the magnitude and timing of the transient hyperemia associated with SD. However, when LSCI was used to visualize the spatial extent of the blood flow changes during SD, a transient but delayed blood flow increase was discovered in the dural vessels overlying the cortex.[67] By imaging the blood flow response within the middle meningeal artery (see Fig. 6), Bolay et al. were able to map the nerve pathway linking the triggering event of a headache (spreading depression) to the subsequent headache.[67] These types of studies were not possible with methods such as laser Doppler or MRI-based techniques that lack sufficient spatial resolution to resolve blood flow in single vessels.

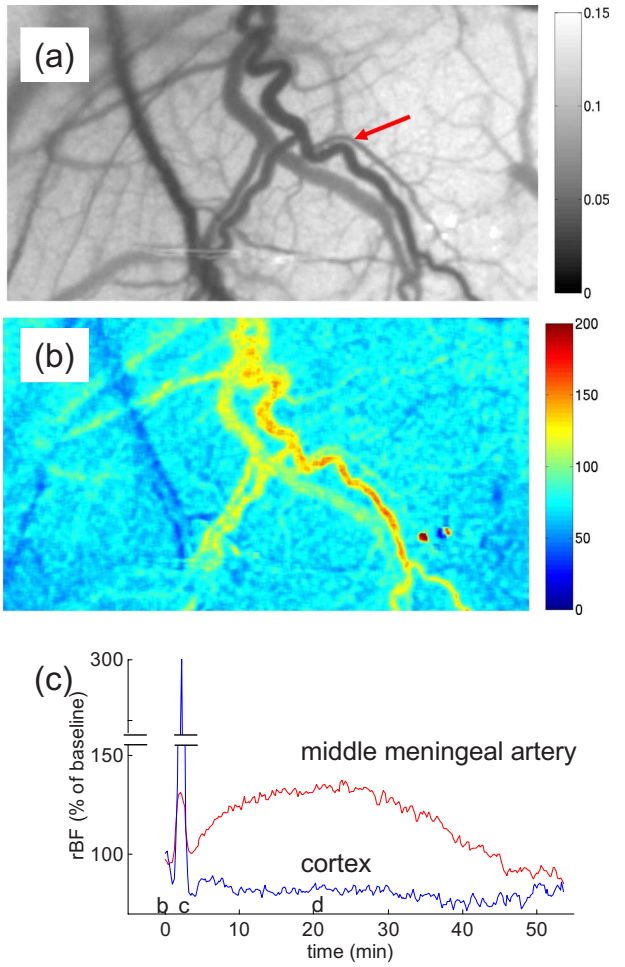

Fig. 6 Blood flow images following cortical spreading depression: (a) the speckle contrast image reveals vasculature in the cortex and dura, the middle meningeal artery is indicated by the arrow; (b) relative blood flow 20 min after induction of cortical SD reveals elevated blood flow in the middle meningeal artery; and (c) time course of the changes in blood flow in the cortex and the middle meningeal artery demonstrating the long-lasting blood flow increase that is restricted to the dural vessel. Reproduced from Ref. 67 with permission.

LSCI has also been used to investigate other aspects of SD such as the difference in hemodynamic response between rats and mice.[68] These studies also demonstrated that LSCI can be performed through an intact skull in mice since the skulls of mice are relatively thin. As in functional activation studies, LSCI has been combined with other imaging methods for multiparameter measurements of the hemodynamic and metabolic responses to SD. Sakadzic et al.[21] investigated the blood flow and oxygenation changes during cortical spreading depression (CSD) using combined LSCI and phosphorescence-quenching measurements, while another recent study[23] combined LSCI with voltage-sensitive dyes to simultaneously measure the hemodynamic (blood flow) and neuronal re-

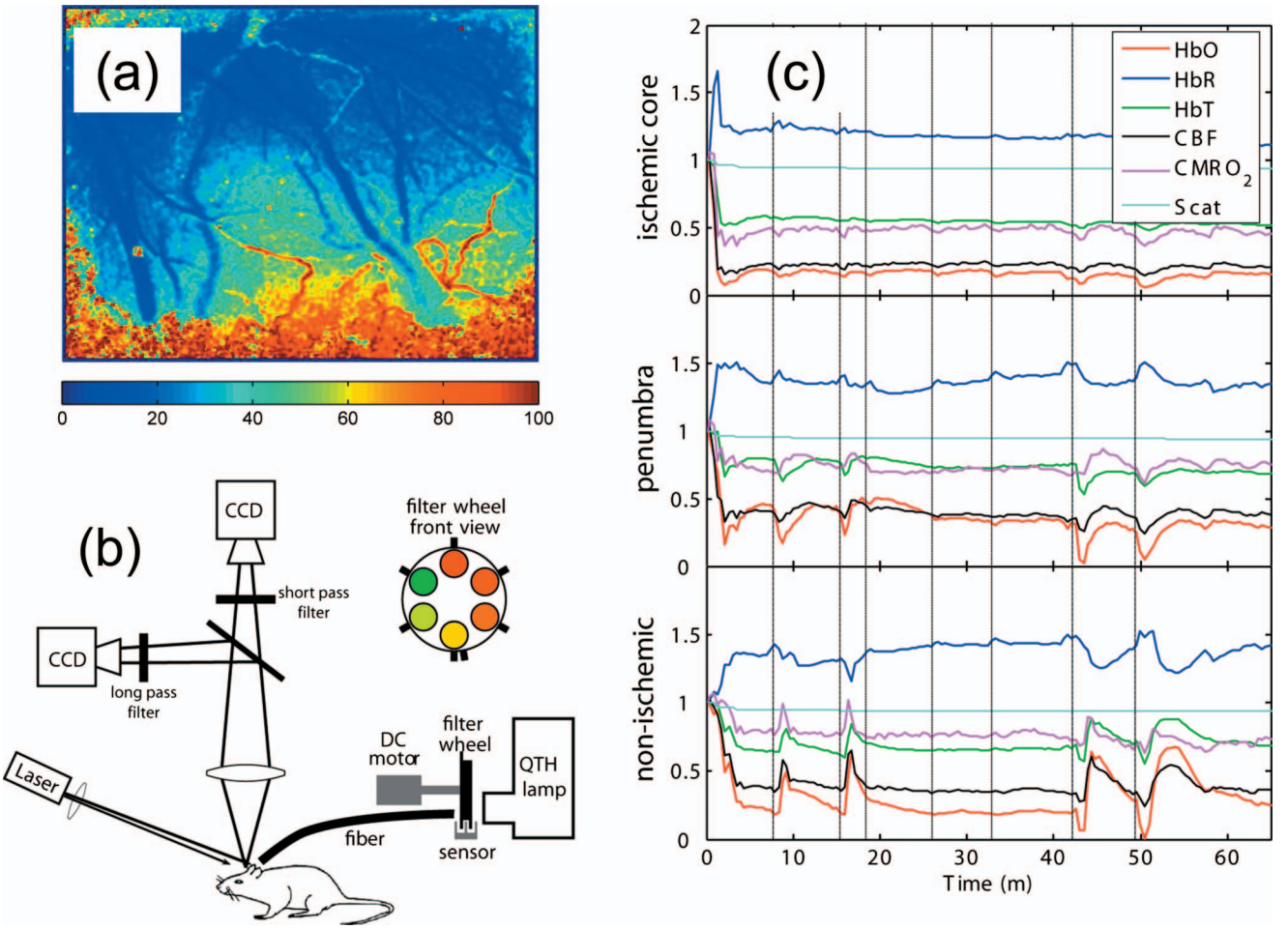

Fig. 7 Application of LSCI to cerebral ischemia: (a) the spatial blood flow gradient following occlusion of an artery can be visualized using LSCI, where the middle cerebral artery was occluded just outside the top region of the image and the color map shows the relative blood flow, expressed as a percentage of preischemic flow; (b) LSCI and MSRI can be performed simultaneously to image multiple hemodynamic parameters; and (c) time courses of changes in oxyhemoglobin (HbO), deoxyhemoglobin (HbR), total hemoglobin (HbT), blood flow (CBF), oxygen consumption ($CMRO_2$), and scattering during a stroke. The three graphs demonstrate the changes in each of these parameters in three spatial regions (ischemic core, penumbra, and nonischemic cortex). (b) and (c) reproduced from Ref. 59 with permission.

sponse to CSD. This combination could be very significant in future studies of neurovascular coupling.

3.3.3 *Stroke*

Animal models of stroke are widely used to investigate the basic pathophysiology of stroke and to evaluate new stroke therapies. A critical aspect of these studies is monitoring of blood flow dynamics in the brain. Laser Doppler flowmetry has been used for many years in such studies and is widely considered to be the gold standard for quantifying blood flow changes in the brain in animal models of stroke. Although MRI and positron emission tomography have also been used in animal models of stroke, the spatial and temporal resolution of these techniques is usually not sufficient to enable detailed studies of blood flow dynamics. LSCI has emerged as a powerful technique for quantifying both the spatial and temporal blood flow changes during stroke due to its high spatial and temporal resolution.[11,63,69–71]

During ischemic stroke, blood flow is reduced in a localized region of the brain leading to a cascade of cellular and molecular events that ultimately results in tissue damage. Blood flow in the area closest to the affected region (ischemic core) is typically reduced to less than 20% of its baseline value, and as a result neurons depolarize and die rapidly. In the region between the ischemic core and the normal tissue (penumbra), neurons preserve the ability to maintain ion homeostasis but are considered to be electrically silent since evoked potentials and spontaneous electrical activity cease.[72] The reduction in blood flow in the penumbra is not as severe as in the core since collateral blood supply to the area is maintained. This reduction in flow in the penumbra can lead to secondary effects such as peri-infarct spreading depolarizations, inflammation, and ultimately cell death.[73] The penumbra has been a primary target of treatment strategies since membrane function is preserved in cells in the penumbra. Restoration of blood flow to the penumbra, therefore, may provide a means of salvaging tissue without loss of function.

Since the ischemic penumbra varies both spatially and temporally, LSCI is one of the few techniques that can provide a dynamic view of the penumbra, as well as the ischemic core and nonischemic areas. LSCI has been used to visualize the CBF changes throughout the ischemic territory in stroke

models in mice, rats, and cats.[11,64,69,74] Figure 7(a) shows an example of the spatial gradient in blood flow following occlusion of the middle cerebral artery in a rat. Closest to the occlusion site, blood flow is reduced to less than 20% of preischemic values and the blood flow deficit gradually improves with distance away from the site of occlusion due to collateral blood flow.

One of the mechanisms that may lead to cell death in the penumbra is the presence of periinfarct depolarizations (PIDs), which resemble the spreading depressions of Leao.[60] PIDs are spontaneously generated following an ischemic insult. As the frequency of PIDs increases, the extent of the ischemic injury has been found to increase as well.[73] Due to the increased metabolic demand, hemodynamic changes occur during PIDs, and LSCI has been used to quantify the CBF changes during PIDs to investigate their role in the evolution of the ischemic infarct.[59,64,69] Since PIDs involve a complex sequence of hemodynamic, metabolic, and neuronal changes, it is particularly beneficial to combine LSCI with other techniques such as MSRI.

Figure 7(c) illustrates the time course of the hemodynamic changes in a mouse stroke model that were acquired with a combined LSCI and MSRI system illustrated schematically[59] in Figure 7(b). Average changes in each hemodynamic parameter within the core (top plot), penumbra (middle plot), and nonischemic cortex (bottom plot) reveal a complex pattern of hemodynamic changes that varies considerably between each hemodynamic parameter and across areas of the cortex. The spatial heterogeneity of these changes highlights the necessity for full-field imaging of each of the hemodynamic parameters. Spontaneous and repetitive PIDs are observed, altering the hemodynamic parameters and oxygen consumption ($CMRO_2$), which can be calculated from the changes in CBF and hemoglobin concentrations.[54] The vertical dashed lines indicate the presence of PIDs. In the nonischemic cortex and penumbra, each PID is accompanied by a drop in all parameters except HbR, followed by a transient overshoot. In the ischemic core, a decrease is observed with no discernable overshoot, suggesting that a small amount of metabolism is taking place even in the most severely ischemic core as evidenced by a further reduction of $CMRO_2$ during a PID. These results illustrate the great potential for imaging of the complex hemodynamic changes that occur during ischemia.

4 Summary

Although LSCI has been used for more than 25 yr, the basic approach has remained relatively unchanged. Over the past decade, LSCI has emerged as a very powerful technique for visualizing flow changes with excellent spatial and temporal resolution. This property combined with relatively simple instrumentation, has resulted in rapid adoption of LSCI, particularly in neuroscience. Despite the simplicity of LSCI, one of the greatest challenges in the future will be to improve the quantitative accuracy of LSCI through approaches such as MSRI. However, significant work is still required to improve our understanding of the complex physics underlying speckle imaging.

Acknowledgments

The authors acknowledge Sean Kirkpatrick, Donald Duncan, and Shuai Yuan for insightful discussions that improved the quality of this manuscript, thank Bernard Choi for providing Fig. 4, and acknowledge support from the National Institutes of Health (NIH) Grants P50-NS010828, P01-NS055104, R01-NS057476, the American Heart Association (Grant No. 0735136N), and the National Science Foundation (Grant No. CBET/0737731).

References

1. H. Cummins and H. L. Swinney, "Light beating spectroscopy," in *Progress in Optics*, E. Wolf, Ed., Vol. VIII, p. 133, North Holland Publishing Co., Amsterdam (1970).
2. R. Pecora, "Quasi-elastic light scattering from macromolecules," *Annu. Rev. Biophys. Bioeng.* **1**, 257–276 (1972).
3. C. Riva, B. Ross, and G. B. Benedek, "Laser Doppler measurements of blood flow in capillary tubes and retinal arteries," *Invest. Ophthalmol.* **11**, 936–944 (1972).
4. M. D. Stern, "In vivo evaluation of microcirculation by coherent light scattering," *Nature (London)* **254**, 56–58 (1975).
5. P. J. Berne and R. Pecora, *Dynamic Light Scattering*, Wiley, New York (1976).
6. R. Bonner and R. Nossal, "Model for laser Doppler measurements of blood flow in tissue," *Appl. Opt.* **20**, 2097–2107 (1981).
7. D. J. Pine, D. A. Weitz, P. M. Chaikin, and E. Herbolzheimer, "Diffusing-wave spectroscopy," *Phys. Rev. Lett.* **60**, 1134–1137 (1988).
8. T. J. Essex and P. O. Byrne, "A laser Doppler scanner for imaging blood flow in skin," *J. Biomed. Eng.* **13**, 189–194 (1991).
9. K. Wardell, A. Jakobsson, and G. E. Nilsson, "Laser Doppler perfusion imaging by dynamic light scattering," *IEEE Trans. Biomed. Eng.* **40**, 309–316 (1993).
10. A. F. Fercher and J. D. Briers, "Flow visualization by means of single-exposure speckle photography," *Opt. Commun.* **37**, 326–330 (1981).
11. A. K. Dunn, H. Bolay, M. A. Moskowitz, and D. A. Boas, "Dynamic imaging of cerebral blood flow using laser speckle," *J. Cereb. Blood Flow Metab.* **21**, 195–201 (2001).
12. R. Bandyopadhyay, A. S. Gittings, S. S. Suh, P. K. Dixon, and D. J. Durian, "Speckle-visibility spectroscopy: a tool to study time-varying dynamics," *Rev. Sci. Instrum.* **76**, 093110 (2005).
13. A. B. Parthasarathy, W. J. Tom, A. Gopal, X. Zhang, and A. K. Dunn, "Robust flow measurement with multi-exposure speckle imaging," *Opt. Express* **16**, 1975–1989 (2008).
14. S. Yuan, "Sensitivity, noise and quantitative model of laser speckle contrast imaging," PhD thesis, Tufts University, Medford, MA (2008).
15. P. Li, S. Ni, L. Zhang, S. Zeng, and Q. Luo, "Imaging cerebral blood flow through the intact rat skull with temporal laser speckle imaging," *Opt. Lett.* **31**, 1824–1826 (2006).
16. S. J. Kirkpatrick, D. D. Duncan, and E. M. Wells-Gray, "Detrimental effects of speckle-pixel size matching in laser speckle contrast imaging," *Opt. Lett.* **33**, 2886–2888 (2008).
17. D. D. Duncan, S. J. Kirkpatrick, and R. K. Wang, "Statistics of local speckle contrast," *J. Opt. Soc. Am. A Opt. Image Sci. Vis* **25**, 9–15 (2008).
18. W. J. Tom, A. Ponticorvo, and A. K. Dunn, "Efficient processing of laser speckle contrast images," *IEEE Trans. Med. Imaging* **27**, 1728–1738 (2008).
19. S. Liu, P. Li, and Q. Luo, "Fast blood flow visualization of high-resolution laser speckle imaging data using graphics processing unit," *Opt. Express* **16**, 14321–14329 (2008).
20. A. K. Dunn, A. Devor, H. Bolay, M. L. Andermann, M. A. Moskowitz, A. M. Dale, and D. A. Boas, "Simultaneous imaging of total cerebral hemoglobin concentration, oxygenation, and blood flow during functional activation," *Opt. Lett.* **28**, 28–30 (2003).
21. S. Sakadzic, S. Yuan, E. Dilekoz, S. Ruvinskaya, S. A. Vinogradov, C. Ayata, and D. A. Boas, "Simultaneous imaging of cerebral partial pressure of oxygen and blood flow during functional activation and cortical spreading depression," *Appl. Opt.* **48**, D169–77 (2009).
22. Z. Luo, Z. Yuan, Y. Pan, and C. Du, "Simultaneous imaging of cor-

tical hemodynamics and blood oxygenation change during cerebral ischemia using dual-wavelength laser speckle contrast imaging," *Opt. Lett.* **34**, 1480–1482 (2009).
23. T. P. Obrenovitch, S. Chen, and E. Farkas, "Simultaneous, live imaging of cortical spreading depression and associated cerebral blood flow changes, by combining voltage-sensitive dye and laser speckle contrast methods," *Neuroimage* **45**, 68–74 (2009).
24. J. D. Briers and S. Webster, "Laser speckle contrast analysis (LASCA): a nonscanning, full-field technique for monitoring capillary blood flow," *J. Biomed. Opt.* **1**, 174–179 (1996).
25. H. Cheng, Q. Luo, S. Zeng, S. Chen, J. Cen, and H. Gong, "Modified laser speckle imaging method with improved spatial resolution," *J. Biomed. Opt.* **8**, 559–564 (2003).
26. K. R. Forrester, J. Tulip, C. Leonard, C. Stewart, and R. C. Bray, "A laser speckle imaging technique for measuring tissue perfusion," *IEEE Trans. Biomed. Eng.* **51**, 2074–2084 (2004).
27. J. W. Goodman, "Statistical properties of laser speckle patterns," in *Laser Speckle and Related Phenomena*, J. C. Dainty, Ed., pp. 9–75, Springer-Verlag, Berlin (1975).
28. D. D. Duncan and S. J. Kirkpatrick, "Can laser speckle flowmetry be made a quantitative tool?" *J. Opt. Soc. Am. A Opt. Image Sci. Vis* **25**, 2088–2094 (2008).
29. J. C. Ramirez-San-Juan, R. Ramos-Garcia, I. Guizar-Iturbide, G. Martinez-Niconoff, and B. Choi, "Impact of velocity distribution assumption on simplified laser speckle imaging equation," *Opt. Express* **16**, 3197–3203 (2008).
30. P. A. Lemieux and D. J. Durian, "Investigating non-Gaussian scattering processes by using nth-order intensity correlation functions," *J. Opt. Soc. Am. A* **16**, 1651–1664 (1999).
31. T. Bellini, M. A. Glaser, N. A. Clark, and V. Degiorgio, "Effects of finite laser coherence in quasielastic multiple scattering," *Phys. Rev. A* **44**, 5215–5223 (1991).
32. H. Cheng, Y. Yan, and T. Q. Duong, "Temporal statistical analysis of laser speckle images and its application to retinal blood-flow imaging," *Opt. Express* **16**, 10214–10219 (2008).
33. S. Yuan, A. Devor, D. A. Boas, and A. K. Dunn, "Determination of optimal exposure time for imaging of blood flow changes with laser speckle contrast imaging," *Appl. Opt.* **44**, 1823–1830 (2005).
34. J. W. Goodman, *Statistical Optics*, Wiley & Sons, New York (1985).
35. P. Zakharov, A. Volker, A. Buck, B. Weber, and F. Scheffold, "Quantitative modeling of laser speckle imaging," *Opt. Lett.* **31**, 3465–3467 (2006).
36. M. Le Thinh, J. S. Paul, H. Al-Nashash, A. Tan, A. R. Luft, F. S. Sheu, and S. H. Ong, "New insights into image processing of cortical blood flow monitors using laser speckle imaging," *IEEE Trans. Med. Imaging* **26**, 833–842 (2007).
37. J. D. Briers and A. F. Fercher, "Retinal blood-flow visualization by means of laser speckle photography," *Invest. Ophthalmol. Visual Sci.* **22**, 255–259 (1982).
38. Y. Tamaki, M. Araie, E. Kawamoto, S. Eguchi, and H. Fujii, "Noncontact, two-dimensional measurement of retinal microcirculation using laser speckle phenomenon," *Invest. Ophthalmol. Visual Sci.* **35**, 3825–3834 (1994).
39. B. Choi, N. M. Kang, and J. S. Nelson, "Laser speckle imaging for monitoring blood flow dynamics in the in vivo rodent dorsal skin fold model," *Microvasc. Res.* **68**, 143–146 (2004).
40. B. Choi, J. C. Ramirez-San-Juan, J. Lotfi, and J. Stuart Nelson, "Linear response range characterization and in vivo application of laser speckle imaging of blood flow dynamics," *J. Biomed. Opt.* **11**, 041129 (2006).
41. Y. C. Huang, T. L. Ringold, J. S. Nelson, and B. Choi, "Noninvasive blood flow imaging for real-time feedback during laser therapy of port wine stain birthmarks," *Lasers Surg. Med.* **40**, 167–173 (2008).
42. Y. Tamaki, M. Araie, E. Kawamoto, S. Eguchi, and H. Fujii, "Noncontact, two-dimensional measurement of tissue circulation in choroid and optic nerve head using laser speckle phenomenon," *Exp. Eye Res.* **60**, 373–383 (1995).
43. T. Sugiyama, Y. Mashima, Y. Yoshioka, H. Oku, and T. Ikeda, "Effect of unoprostone on topographic and blood flow changes in the ischemic optic nerve head of rabbits," *Arch. Ophthalmol. (Chicago)* **127**, 454–459 (2009).
44. N. Koseki, M. Araie, A. Tomidokoro, M. Nagahara, T. Hasegawa, Y. Tamaki, and S. Yamamoto, "A placebo-controlled 3-year study of a calcium blocker on visual field and ocular circulation in glaucoma with low-normal pressure," *Ophthalmology* **115**, 2049–2057 (2008).
45. K. Yaoeda, M. Shirakashi, S. Funaki, H. Funaki, T. Nakatsue, and H. Abe, "Measurement of microcirculation in the optic nerve head by laser speckle flowgraphy and scanning laser Doppler flowmetry," *Am. J. Ophthalmol.* **129**, 734–739 (2000).
46. H. Isono, S. Kishi, Y. Kimura, N. Hagiwara, N. Konishi, and H. Fujii, "Observation of choroidal circulation using index of erythrocytic velocity," *Arch. Ophthalmol. (Chicago)* **121**, 225–231 (2003).
47. N. Konishi, Y. Tokimoto, K. Kohra, and H. Fujii, "New laser speckle flowgraphy system using CCD camera," *Opt. Rev.* **9**, 163–169 (2002).
48. C. T. W. Moonen and P. A. Bandettini, Eds., *Functional MRI*, Springer-Verlag, Berlin (1999).
49. A. Grinvald, E. Lieke, R. D. Frostig, C. D. Gilbert, and T. N. Wiesel, "Functional architecture of cortex revealed by optical imaging of intrinsic signals," *Nature (London)* **324**, 361–364 (1986).
50. S. A. Masino and R. D. Frostig, "Quantitative long-term imaging of the functional representation of a whisker in rat barrel cortex," *Proc. Natl. Acad. Sci. U.S.A.* **93**, 4942–4947 (1996).
51. S. A. Masino, M. C. Kwon, Y. Dory, and R. D. Frostig, "Characterization of functional organization within rat barrel cortex using intrinsic signal optical imaging through a thinned skull," *Proc. Natl. Acad. Sci. U.S.A.* **90**, 9998–10002 (1993).
52. D. Y. Ts'o, R. D. Frostig, E. E. Lieke, and A. Grinvald, "Functional organization of primate visual cortex revealed by high resolution optical imaging," *Science* **249**, 417–420 (1990).
53. J. Mayhew, D. Johnston, J. Berwick, M. Jones, P. Coffey, and Y. Zheng, "Spectroscopic analysis of neural activity in brain: increased oxygen consumption following activation of barrel cortex," *Neuroimage* **13**, 540–543 (2001).
54. A. K. Dunn, A. Devor, A. M. Dale, and D. A. Boas, "Spatial extent of oxygen metabolism and hemodynamic changes during functional activation of the rat somatosensory cortex," *Neuroimage* **27**, 279–290 (2005).
55. B. Weber, C. Burger, M. T. Wyss, G. K. von Schulthess, F. Scheffold, and A. Buck, "Optical imaging of the spatiotemporal dynamics of cerebral blood flow and oxidative metabolism in the rat barrel cortex," *Eur. J. Neurosci.* **20**, 2664–2670 (2004).
56. T. Durduran, M. G. Burnett, G. Yu, C. Zhou, D. Furuya, A. G. Yodh, J. A. Detre, and J. H. Greenberg, "Spatiotemporal quantification of cerebral blood flow during functional activation in rat somatosensory cortex using laser-speckle flowmetry," *J. Cereb. Blood Flow Metab.* **24**, 518–525 (2004).
57. B. M. Ances, D. F. Wilson, J. H. Greenberg, and J. A. Detre, "Dynamic changes in cerebral blood flow, O_2 tension, and calculated cerebral metabolic rate of O_2 during functional activation using oxygen phosphorescence quenching," *J. Cereb. Blood Flow Metab.* **21**, 511–516 (2001).
58. A. Devor, E. M. Hillman, P. Tian, C. Waeber, I. C. Teng, L. Ruvinskaya, M. H. Shalinsky, H. Zhu, R. H. Haslinger, S. N. Narayanan, I. Ulbert, A. K. Dunn, E. H. Lo, B. R. Rosen, A. M. Dale, D. Kleinfeld, and D. A. Boas, "Stimulus-induced changes in blood flow and 2-deoxyglucose uptake dissociate in ipsilateral somatosensory cortex," *J. Neurosci.* **28**, 14347–14357 (2008).
59. P. B. Jones, H. K. Shin, D. A. Boas, B. T. Hyman, M. A. Moskowitz, C. Ayata, and A. K. Dunn, "Simultaneous multispectral reflectance imaging and laser speckle flowmetry of cerebral blood flow and oxygen metabolism in focal cerebral ischemia," *J. Biomed. Opt.* **13**, 044007 (2008).
60. A. Leao, "Spreading depression of activity in the cerebral cortex," *J. Neurophysiol.* **7**, 359–390 (1944).
61. M. Lauritzen, "Pathophysiology of the migraine aura. The spreading depression theory," *Brain* **117**(Pt. 1), 199–210 (1994).
62. G. G. Somjen, "Mechanisms of spreading depression and hypoxic spreading depression-like depolarization," *Physiol. Rev.* **81**, 1065–1096 (2001).
63. A. J. Strong, E. L. Bezzina, P. J. Anderson, M. G. Boutelle, S. E. Hopwood, and A. K. Dunn, "Evaluation of laser speckle flowmetry for imaging cortical perfusion in experimental stroke studies: quantitation of perfusion and detection of peri-infarct depolarisations," *J. Cereb. Blood Flow Metab.* **26**, 645–653 (2006).
64. A. J. Strong, P. J. Anderson, H. R. Watts, D. J. Virley, A. Lloyd, E. A. Irving, T. Nagafuji, M. Ninomiya, H. Nakamura, A. K. Dunn, and R. Graf, "Peri-infarct depolarizations lead to loss of perfusion in ischaemic gyrencephalic cerebral cortex," *Brain* **130**, 995–1008 (2007).
65. J. P. Dreier, J. Woitzik, M. Fabricius, R. Bhatia, S. Major, C. Drenck-

hahn, T. N. Lehmann, A. Sarrafzadeh, L. Willumsen, J. A. Hartings, O. W. Sakowitz, J. H. Seemann, A. Thieme, M. Lauritzen, and A. J. Strong, "Delayed ischaemic neurological deficits after subarachnoid haemorrhage are associated with clusters of spreading depolarizations," *Brain* **129**, 3224–3237 (2006).
66. M. Fabricius, S. Fuhr, R. Bhatia, M. Boutelle, P. Hashemi, A. J. Strong, and M. Lauritzen, "Cortical spreading depression and peri-infarct depolarization in acutely injured human cerebral cortex," *Brain* **129**, 778–790 (2006).
67. H. Bolay, U. Reuter, A. K. Dunn, Z. Huang, D. A. Boas, and M. A. Moskowitz, "Intrinsic brain activity triggers trigeminal meningeal afferents in a migraine model," *Nat. Med.* **8**, 136–142 (2002).
68. C. Ayata, H. K. Shin, S. Salomone, Y. Ozdemir-Gursoy, D. A. Boas, A. K. Dunn, and M. A. Moskowitz, "Pronounced hypoperfusion during spreading depression in mouse cortex," *J. Cereb. Blood Flow Metab.* **24**, 1172–1182 (2004).
69. H. K. Shin, A. K. Dunn, P. B. Jones, D. A. Boas, M. A. Moskowitz, and C. Ayata, "Vasoconstrictive neurovascular coupling during focal ischemic depolarizations," *J. Cereb. Blood Flow Metab.* **26**(8), 1018–1030 (2005).
70. H. K. Shin, A. K. Dunn, P. B. Jones, D. A. Boas, E. H. Lo, M. A. Moskowitz, and C. Ayata, "Normobaric hyperoxia improves cerebral blood flow and oxygenation, and inhibits peri-infarct depolarizations in experimental focal ischaemia," *Brain* **130**, 1631–1642 (2007).
71. S. Zhang and T. H. Murphy, "Imaging the impact of cortical microcirculation on synaptic structure and sensory-evoked hemodynamic responses in vivo," *PLoS Biol.* **5**, e119 (2007).
72. U. Dirnagl, C. Iadecola, and M. A. Moskowitz, "Pathobiology of ischaemic stroke: an integrated view," *Trends Neurosci.* **22**, 391–397 (1999).
73. G. Mies, T. Iijima, and K. A. Hossmann, "Correlation between peri-infarct DC shifts and ischaemic neuronal damage in rat," *NeuroReport* **4**, 709–711 (1993).
74. D. N. Atochin, J. C. Murciano, Y. Gursoy-Ozdemir, T. Krasik, F. Noda, C. Ayata, A. K. Dunn, M. A. Moskowitz, P. L. Huang, and V. R. Muzykantov, "Mouse model of microembolic stroke and reperfusion," *Stroke* **35**, 2177–2182 (2004).